Evidence of a pseudo-mobility-edge for electrons in disordered layers

T. J. Godin
Molecular Science Research Center, Pacific Northwest Laboratory, P.O. Box 999, Richland, Washington 99352

Roger Haydock
Department of Physics and Materials Science Institute, University of Oregon, Eugene, Oregon 97403
(Received 24 May 1991)

We report results of transmittance calculations for current carriers in disordered layers using the block recursion method. This technique transforms a model of an elastic two-dimensional (2D) scattering potential to an "effective quantum circuit" whose transmittance can be readily found. We observe evidence of a "pseudo-mobility-edge": a kink in the inverse localization length as a function of energy. The energy at which this feature occurs is well separated from the band edge, and is observed to depend on the disorder, but not the sample size or geometry. The 2D system's behavior is intermediate between the 3D system's behavior, which is expected to display a true mobility edge, and 1D system's behavior, where localization lengths vary smoothly with energy.

I. INTRODUCTION

The mobility of charge carriers trapped in a disordered layer, and hence the electrical conductance of that layer, depend on the length scale of Anderson localization[1] near the Fermi energy.[2] Since this energy can be varied by doping or gating, it is important to understand how localization lengths vary as a function of carrier energy. Accordingly, localization in eigenstates of a disordered potential is a problem of great interest.

The theory of electron motion in disordered layers underwent a major revision a decade ago. Previously, it was thought that mobility edges, separating extended from localized states, could exist in two-dimensional (2D) potentials. Subsequently, a consensus emerged that all eigenstates of a 2D disordered potential have unit probability of displaying some form of localization. Since then, it has been widely believed that 2D systems display behavior similar to 1D systems, where universal exponential localization, and a smooth variation of localization length with energy, have been proven rigorously.[3]

The more recent view of 2D localization arose in part from single-parameter scaling theory[4] and effective field-theoretical models.[5] These predicted universal exponential localization in 2D systems. Other theories predicted different regimes of exponential and power-law localization for sufficiently weak disorder,[6,7] indicating a transition between weakly and strongly insulative states.

The latter two references, based on perturbative analytic calculations using the recursion method,[8] predicted energies at which such a weak-disorder transition would occur, along with effective carrier masses near the transition. A kink in the inverse localization length as a function of energy was predicted at the same energy, similar to the behavior of tunneling current at energies in a band gap. Such a singularity could occur even if the more weakly insulative states were exponentially localized. These results were not consistent with a single scaling parameter.

Because of the complexity of disordered potentials, analytic work is difficult. Numerical work[9] has therefore been heavily relied upon, despite the difficulty in extrapolating results for finite samples to infinite systems.

In a recent Letter[10] we reported results of calculations of electronic transmittance in elastic, disordered 2D potentials using the block recursion method.[11,12] The results showed evidence of a kink in the inverse localization length as a function of energy, supporting a key result of the analytic recursion work. In finite-sized samples this "pseudo-mobility-edge," a boundary between strongly and weakly localized states, caused a transmittance decrease comparable to that at the band edge of a similar-sized crystalline sample. This behavior is not analogous to either a 3D mobility edge or the smooth variation of localization length in the 1D system. In a sense, however, the behavior of these 2D systems is intermediate between the 1D and 3D cases.

Here, we present these results in more detail, and quantify the properties of this apparent feature.

II. RESULTS OF ANALYTIC RECURSION THEORY

The motion of electrons in the low-temperature, low-current limit can be modeled as single particles acting under the influence of a Hamiltonian operator H which contains an elastic scattering potential. It is often convenient to represent H as a matrix operating on a tight-binding basis of local orbitals. Here, we represent the operator and matrix with the same symbol.

The recursion theory of localization[7] proceeds by changing the basis of H, so that in the acquired basis the matrix is tridiagonal. The transformed matrix thus defines an effective 1D chain model with nearest-neighbor interactions. The eigenstates of the 1D chain are then found and expanded in the original basis vectors. The spatially asymptotic properties of these states can then be studied. This method is exact in principle, although the complexity of disordered systems makes analytic calcula-

tions difficult. Use of a perturbative method allowed calculations valid for weak disorder.

This previous analytic work produced several key results, which we review in this section. In both two and three dimensions, both the diagonal and hopping elements of the chain model converged to stable values as successive acquired basis vectors were generated. In 3D systems, the diagonal elements converged rapidly enough to give extended states (in this weakly disordered regime). However, in 2D systems convergence was slow enough to give power-law localization near the band center. In both cases, the hopping elements converged to a value which gave the chain model an effective band edge, located at an energy different from the band edge of the actual 2D or 3D sample. Carrier transmittance outside the effective band edge would thus behave like tunneling outside the crystalline band, with exponential localization whose length scale L varied as an inverse square root of energy E:

$$T \approx e^{-x/L} , \tag{1a}$$

$$1/L - 1/L_c = \alpha |E - E_c|^{1/2} , \tag{1b}$$

where T is transmittance, x is the sample length, α is constant for a particular disorder strength, E_c is the effective band-edge energy, and L_c is the localization length at E_c. α can be thought of as the square root of an "effective mass" in the strongly localized region. Values for E_c and α as a function of disorder strength were found.

In 3D systems, a metal-insulator transition occurs at E_c. In 2D systems, a transition between exponential and power-law localization was indicated for sufficiently weak disorder. In both cases, for finite-sized samples (1b) indicates a change in transmittance at E_c similar to that in a crystal at the band edge; however, there is no similar singularity in the density of states near E_c.

III. TRANSMITTANCE CALCULATIONS USING THE BLOCK RECURSION METHOD

We now turn to the main topic of this paper; that is, a numerical examination of the issues raised by the earlier weak-disorder analytic theory described in the previous section. A detailed description of transmittance calculations using the block recursion method, as well as example listings of the computer source code, is contained in Refs. 10–12. The features of such a calculation, as well as the model of disordered 2D potentials used, are briefly described below.

We use the Anderson model[1] of an elastic, disordered single-carrier potential. A single basis orbital is localized on each of a set of $N=n^2$ sites arranged in an $n \times n$ 2D square lattice. The orbitals have constant nearest-neighbor hopping integrals v, and energies which are randomly and evenly distributed between $+w/2$ and $-w/2$. The dimensionless parameter w/v thus describes the disorder strength.

Orbitals localized on sites at opposite corners of the sample are coupled via hopping integrals v' to orbitals localized at the ends of semi-infinite 1D periodic leads (Fig. 1). One lead supports an incident and reflected Bloch wave; the other supports a transmitted wave. (v' is usually set to make the bandwidth of the leads larger than that of the sample, so that the entire sample band may be examined.) The projections of these waves on the basis states at the ends of the leads and sample corners provide boundary conditions for a solution of the time-independent Schrödinger equation

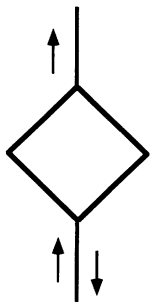

FIG. 1. Lead-sample geometry used. Opposite corners of a square lattice are coupled to semi-infinite 1D leads, through which incident, reflected, and transmitted waves (symbolized here by arrows showing the direction of propagation) can pass.

$$H\psi = E\psi \tag{2}$$

within the sample. Here E is the carrier energy, ψ is an unknown vector, and H is the Hamiltonian operator which describes the model. The block recursion method is an efficient, stable algorithm which can find the relative amplitudes of the transmitted and incident waves for a solution of (2), and hence the transmittance.

The calculation proceeds as follows. Let u_1 be an $N \times 2$ matrix whose two columns are vectors representing, respectively, the basis orbitals at the sample corners. Similarly, let u_0 be an $N \times 2$ matrix whose columns represent the orbitals at the lead ends. We first generate from these a set of $N \times 2$ matrices $\{u_0, u_1, u_2, \ldots, u_{N/2}\}$ which satisfy the recurrence

$$Hu_i = u_{i-1}B_i^\dagger + u_i A_i + u_{i+1}B_{i+1} , \tag{3}$$

where $B_i^\dagger$, A_i, and B_{i+1} are 2×2 matrices. We start with u_0, u_1, and the initial condition

$$B_1^\dagger = u_0^\dagger H u_1 , \quad A_1 = u_1^\dagger H u_1 . \tag{4}$$

By applying H to each u_i and subtracting the u_i and u_{i-1} components from this product, $u_{i+1}B_{i+1}$ is generated and then factored by requiring the columns of u_{i+1} to be mutually orthonormal. A_{i+1} is given by $u_{i+1}^\dagger H u_{i+1}$; the process is repeated by applying H to u_{i+1} and so on.

The columns of the u_i are vectors which form a new basis for H. In this basis the matrix representation of H is block tridiagonal; the A_i are the diagonal blocks, the B_i and $B_i^\dagger$ are, respectively, the subdiagonal and superdiagonal blocks, and all other elements are zero. This matrix also has the feature that the orbitals to which the boundary conditions are applied (those contained in u_0 and u_1) are included in the basis. By applying these boundary conditions, the transmittance T of a solution to (2) is given by the matrix continued fraction

$$T(E) = 4 \sin^2\theta |[e^{i\theta} I - v' G(E)]^{-1}_{\mathrm{OD}}|^2 . \tag{5}$$

θ is the change in phase angle of the transmitted wave be-

tween a corner site and site at the end of a lead, G is the 2×2 submatrix of the resolvent of H spanned by the two corner site orbitals, I is the 2×2 identity matrix and the subscript OD means the off-diagonal element. With the matrix representation of H in block-tridiagonal form, $G(E)$ is found using the matrix continued fraction

$$G(E)=[EI-A_1-B_2^{\dagger}(EI-A_2-\cdots)^{-1}B_2]^{-1}\ . \qquad (6)$$

In practice, near the band edge (where the results described here were obtained) the number of levels needed for the continued fraction to converge is much smaller than the number of degrees of freedom in the sample model.

In the new basis, the block-tridiagonal matrix H is an "effective quantum circuit": a Hamiltonian which represents a simpler model, but one which has the same transmittance at energy E as the original, untransformed matrix.

This method is related to the scalar recursion method.[8] The stability and accuracy of this family of techniques is well understood,[13] and described in detail in Refs. 10 and 12. Briefly, rounding error in the recursion (3) causes a loss of orthogonality in the basis states; however, the nonorthogonal vectors are still a valid basis for the Hamiltonian matrix. This effect thus does not contribute to error in the calculated transmittance. The continued fraction (6) may be evaluated with great numerical stability.

The accuracy can be confirmed by applying the method to an exactly soluble Hamiltonian. For example, the resolvent of a diagonal Hamiltonian matrix can be calculated directly with a spectral formula. However, application of the block recursion transformation to such a matrix involves about as many operations, and as much rounding error, as any sparse matrix. Figures 2 and 3 show results of a block recursion calculation on a diagonal matrix of dimension 1000×1000 at two different energies. The diagonal elements randomly vary between 1.0 and -1.0; two orthogonal vectors (not eigenvectors) were chosen for u_1, the states coupled to leads. Figure 2 shows the inner product of the first columns of u_n and u_0. In an exact calculation, this should equal one for $n=0$, and zero otherwise. However, in the finite-precision calculation this overlap is substantial long before the degrees of freedom have been exhausted. Figure 3 compares an essentially exact calculation of the transmittance using a spectral formula for G to the block recursion result. When a sufficient number of levels are included in the continued fraction, the transmittance sharply converges to within machine precision of the correct value. Note that fewer levels are required further from the band center. This is consistent with experience with the scalar recursion method.

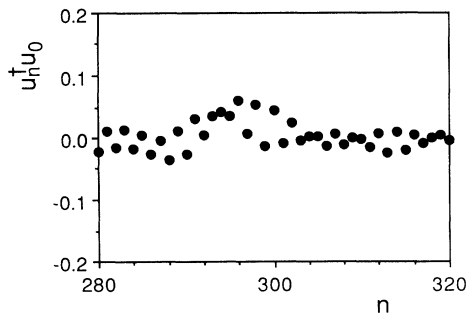

FIG. 2. Overlap of transformed basis vector u_n with starting vector u_0 for the sample calculation described in the text. In an exact calculation, the vectors would be orthogonal; in this finite-precision calculation orthogonality breaks down.

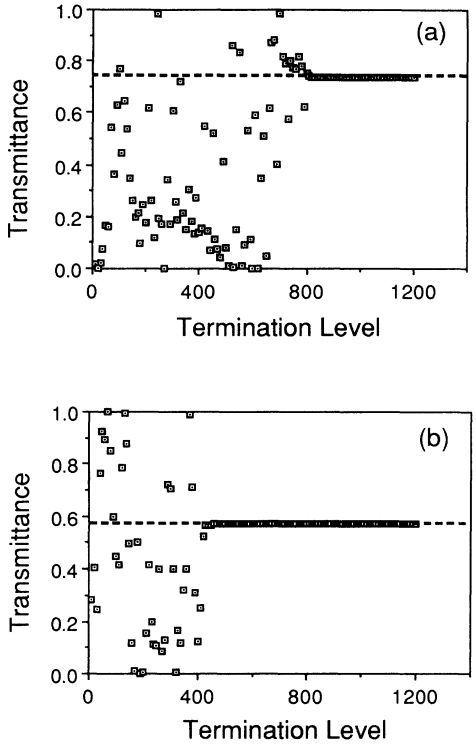

FIG. 3. Comparison of the calculated transmittance to an essentially exact value for sample calculation described in the text. (a) Despite the breakdown in orthogonality of the basis vectors, the transmittance sharply converges to within machine precision of the correct value when a sufficient number of levels are included in the continued fraction. This number is smaller at the energy used in (b), which is further from the band center.

IV. TRANSMITTANCE OF DISORDERED 2D POTENTIALS

This section describes an effect we have observed in disordered 2D potentials, which we call a pseudo-mobility-edge. By that we mean a feature at a particular energy, well separated from the sample band edge and determined only by the sample disorder, at which a finite-sized sample displays a falloff in transmittance similar in appearance to that at a crystal band edge or 3D mobility edge. However, states on both sides are believed to be localized, so that an infinite sample would insulate in both regimes (hence the prefix "pseudo").

We have examined the natural logarithm of transmit-

tance as a function of energy for samples with a wide range of sizes (measured by number of sites n per edge) and disorder strength (measured by the disorder parameter w/v). The behavior shown in Fig. 4, which displays results for several 180×180 site samples of varying disorder, is typical.

To illustrate the properties of the disordered samples, it is first instructive to examine the transmittance of a crystal ($w/v=0$) [Fig. 4(a)]. In this single-band model, a crystal has extended states at energies between the band edges at $+4v$ and $-4v$. In this region, the transmittance is large. It is not unity, however, and it is important to distinguish the reflective features at work here from those caused by localization. The 1D leads act as point sources and receivers of waves, causing a power-law decay of the transmittance with sample size. Reflection occurs at the sample edges. The boundary conditions at the edges also constrain the transverse wave vector; this limits the available phase space for transmission from the 1D leads, which have no similar constraints. This latter "mismatch" between lead and sample causes sharp resonances where an incident wave is close in energy to an allowed sample state. All of these effects exist, of course, in the disordered samples as well; for finite samples with relatively weak localization they are likely to be more important than localization effects.

Conversely, the transmitted intensity is relatively small outside the band. Incident states with energies outside

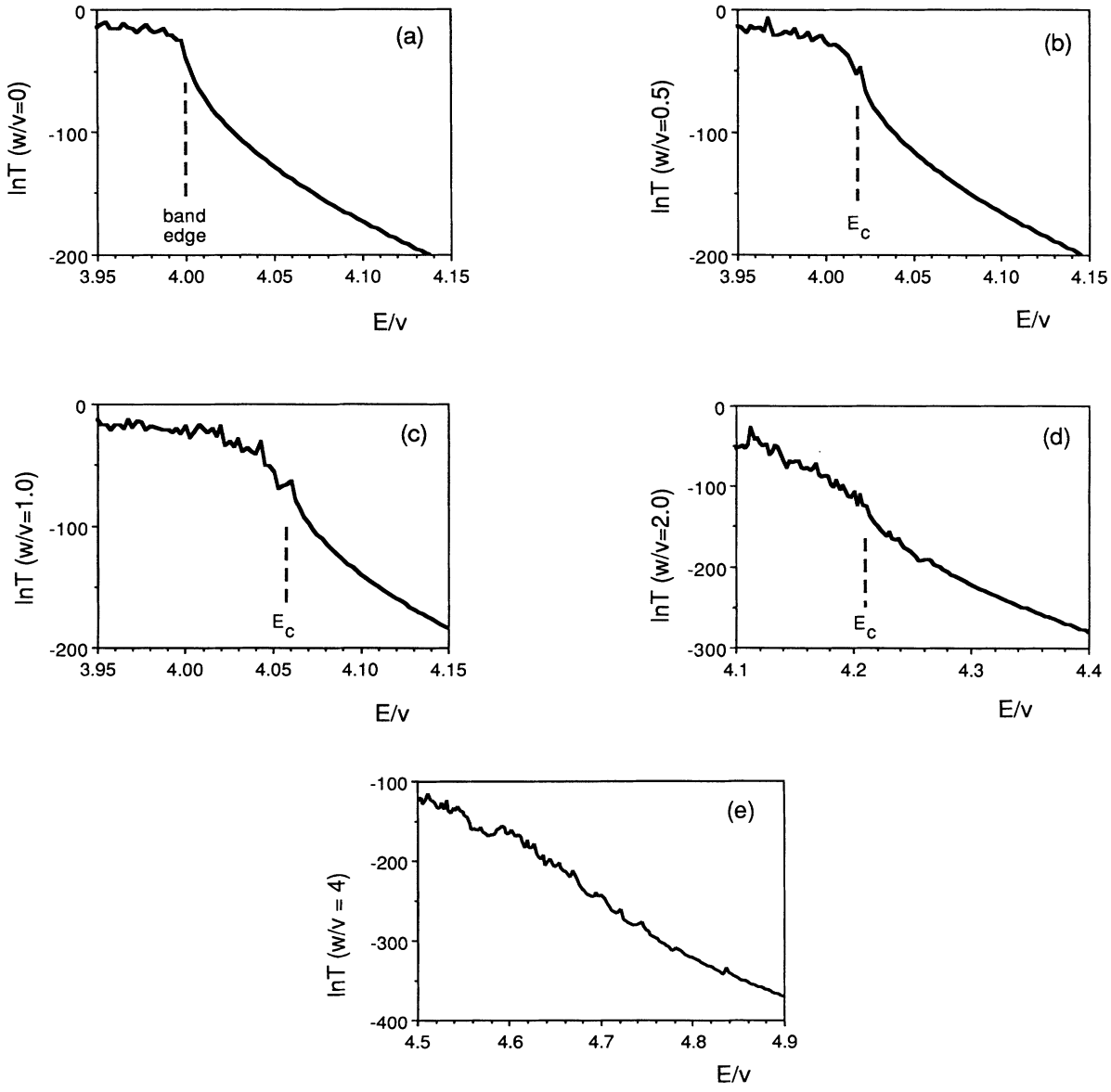

FIG. 4. ln transmittance of single 2D samples with w/v equal to (a) 0.0 (a crystal); (b) 0.5; (c) 1.0; (d) 2.0; and (e) 4.0. The crystal band edge in (a) is marked with a dashed line. Note the feature [marked with dashed lines in (b)–(d)] that appears similar to the crystalline band edge and shows up distinctly in the lower-disorder samples. This feature is, however, well separated from the true band edge. When the disorder increases [as in (e)] the feature becomes less distinct in single samples.

the band evanescently decay with a length scale proportional to the square root of the difference in energy from the band-edge energy. The transmittance thus does not fall sharply to zero, but displays a singularity (kink) at the band edge. These are all, of course, results of elementary band theory.

Figure 4(b) shows a similar-sized sample with some disorder ($w/v=0.5$) introduced. Now at $E=4.02v$, a falloff of transmittance, similar in appearance to that at the crystal band edge, occurs. We denote this energy as E_c. The band edge of this sample, however, is given by Lifschitz[14] as $E_L=4v+w/2$, or $4.25v$. There is no singularity similar to the band edge in the density of states at E_c, nor is there any singularity in the transmittance at the band-edge energy E_L. As the disorder increases [Figs. 4(c) and 4(d)], the transmittance near the band center decreases, but a similar steep falloff occurs. Finally, for sufficient disorder [Fig. 4(e)] the feature is no longer obvious (but reappears when results from many samples are averaged, as described below).

The location of E_c appears to depend only on the disorder strength. For different samples of the same size and disorder, the observed E_c varies only by an amount comparable to the root-mean-square deviation of the site energy, divided by the number of sites in the sample. Because of statistical fluctuations in the random sets of site energies, this is the minimum variation that can be expected. Furthermore, the location of E_c is not observed to depend on sample size or geometry, or alternate lead arrangements (such as variation of v' or connecting leads to edge midpoints). When these are varied, details of the transmittance (such as the locations of the lead-sample "mismatch" resonances) change; however, E_c remains the same (in the sense defined above).

These results appear qualitatively consistent with the prediction of an effective band edge from analytic recursion theory. Quantitative agreement can be tested by fitting the data in Figs. 4(a) and 4(b) to Eq. (1). If we presume that the states decay exponentially, then

$$\ln T(E)\approx -x/L(E)\ , \tag{7}$$

where x is a distance between leads. Substituting into (1) leads to the equation

$$[1/\ln T(E_c)-1/\ln T(E)]^2\approx \text{const}\times|E_c-E| \tag{8}$$

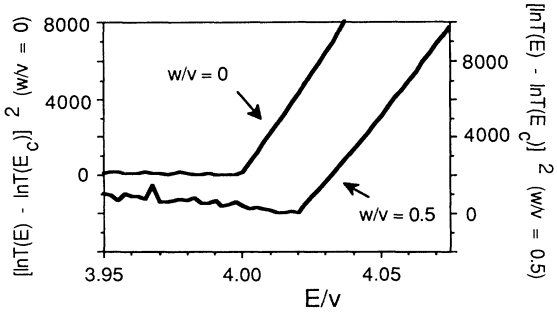

FIG. 5. Data from Figs. 4(a) and 4(b), rescaled to display effective band-edge behavior. The axes are staggered to make the two curves distinct below E_c.

if E_c is the effective band-edge energy.

Figure 5 shows the same data as Figs. 4(a) and 4(b) scaled in this fashion. For the crystal, E_c is taken to be the band-edge energy. Note that in both cases, there are two regimes: roughly constant transmittance below E_c, and an excellent agreement with square-root behavior above. Note again, however, that in the disordered case this feature is well separated from the band edge. There are plenty of allowed states above E_c; they are simply far more insulative than those below.

At higher disorders (e.g., $w/v=4$) there is a similar changeover to such a square-root dependence. This can be seen by a more rigorous measurement of the localization length by finding the scaling of the transmittance averaged over many samples. Figure 6(a) shows data for samples ranging in size from 20 to 180 sites square at two energies. The scaling variables are designed to separate exponential decay from the power-law decay caused by the 1D lead arrangement. The slopes of the lines equal the exponential localization length. (Larger abscissas correspond to larger samples, larger ordinates to larger transmittances. x is the distance between leads, measured in lattice spacings.) Data points represent the mean, and error bars the standard errors, of the scaling variables. The results for many different energies at $w/v=4$ are shown in Fig. 6(b).

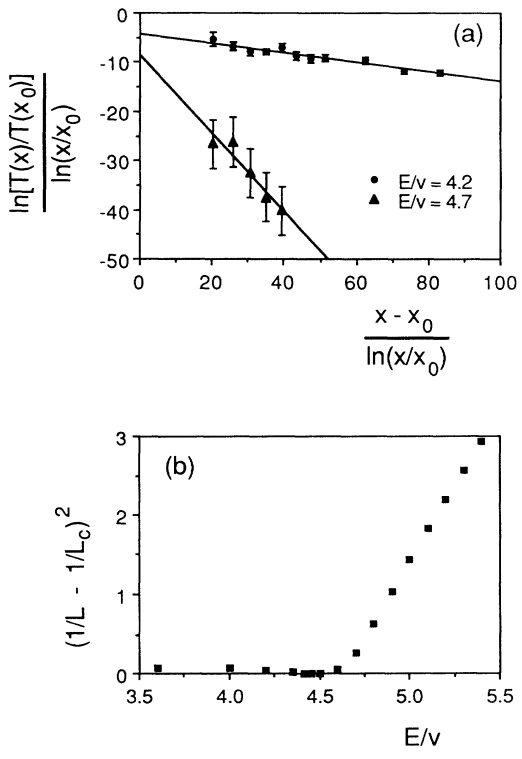

FIG. 6. (a) Variation of transmittance with sample size for $w/v=4.0$. The scaling variables are designed to remove power-law decay arising from the sample geometry; the slopes of the lines equal exponential localization lengths (see text). (b) Localization lengths from scaling graphs at various energies for $w/v=4.0$. The results are scaled to test square-root dependence on energy as described in text.

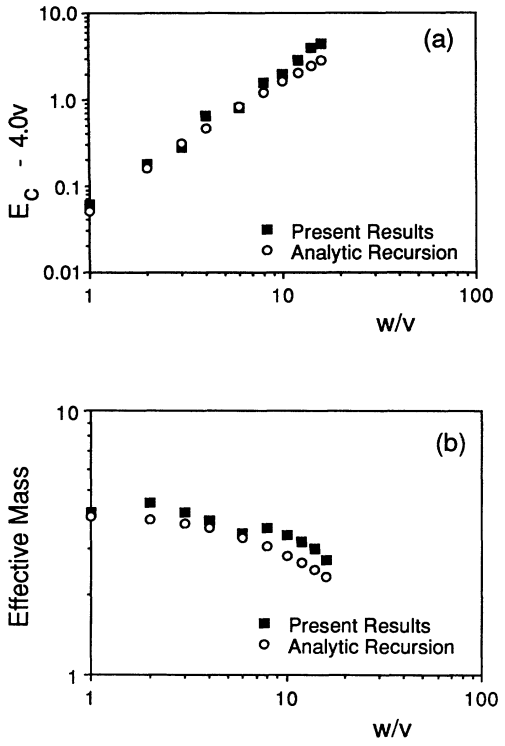

FIG. 7. Comparison of numerically observed values of (a) E_c and (b) carrier effective mass compared to results of analytic recusion theory.

Note again the characteristic changeover in behavior, despite the fact that states on both sides of E_c clearly display exponential localization. This is strong evidence that the feature is not a true metal-insulator transition, which is expected in 3D systems but not in 2D systems. Rather, this is a change from weakly to strongly insulative states.

In Fig. 6(b), the feature appears rounded. This is caused by the aforementioned statistical fluctuations between samples. Because of the unavoidable variation in E_c from one sample to another, at energies near the feature each average will include some data from samples for which E is slightly less than, and some slightly greater than, E_c. These statistical fluctuations are also apparent in the error bars on the scaling graph. At energies greater than E_c the standard error is much larger, even though the averages show negligible deviation from a straight line. This is because a fluctuation in the location of E_c will cause a much greater transmittance change in this region, where T depends so critically on the distance in energy from E_c.

For highly disordered samples, the part of Fig. 6(b) above E_c (where the localization length varies as a square root) provides a means of measuring the location of E_c (the intercept of the line) and the effective mass of carriers (the slope of the line) in this regime. These are compared to the predictions of the analytic recursion model[7] with no adjustable parameters (Fig. 7). Each data point in Fig. 7 was obtained from a graph of sample-averaged localization lengths like Fig. 6. It should be noted that the analytic results were valid in the asymptotic limit of weak disorder. All disorder strengths used in this study are substantial by comparison. However, we observe agreement with these results, particularly for the lower disorders used ($w/v < 3$).

The analytic recursion theory also predicted that states on the less insulative side of E_c would be power-law localized for sufficiently weak disorder. We are unable at this time to examine samples of sufficient size to make accurate measurements of scaling in such a weakly localized regime, and are thus unable to test this claim.

V. CONCLUSION

We have found evidence that an effective band edge, predicted by analytic recursion results, exists in 2D disordered potentials. This is characterized by a falloff in the transmittance at an energy E_c, whose location depends only on the disorder strength. Unlike a crystal, however, this does not signify a change from metallic to insulating behavior, since states on both sides of the feature are observed to be exponentially localized. Also, the apparent kink in the transmittance does not occur at the band edge as in the crystal. The far weaker transmittance on one side of E_c thus is not caused by evanescent decay in a forbidden region, but a much higher degree of Anderson localization in a region where the density of states is still substantial.

For finite samples, this "pseudo-mobility-edge" behaves similarly to a mobility edge. It is clearly a qualitatively different feature, however, since it is a transition between localized regimes. It is also distinct from the 1D case, in which universal exponential localization and a smooth variation of localization length with energy have been proven.[3] In a sense, then, the behavior of the 2D system is intermediate between the 1D and 3D cases.

Lower-resolution studies have indicated a similar functional falloff in $1/L$ near the crystal band edge in disordered systems.[15] However, we are not aware of any previous numerical evidence for such a kink in $1/L$ in 2D systems. Other studies[9] have examined much higher disorder strengths, or have not extended sufficiently into the band tails, or have not been sufficiently energy resolved. In appropriate regimes of energy and disorder, we obtain results consistent with those of these authors. A detailed description of previous studies and their relation to the block recursion approach is provided in the references.[11]

ACKNOWLEDGMENTS

This work was supported by National Science Foundation Condensed Matter Theory Grant No. DMR-90-22525, Binational Science Foundation Grant No. BSF-85-00373, and equipment grants from the Convex Computer Corporation. Pacific Northwest Laboratory is operated for the U.S. Department of Energy by Battelle Memorial Institute under Contract No. DE-AC06-76RLO 1830.

[1]P. W. Anderson, Phys. Rev. **109**, 1492 (1958).
[2]N. F. Mott and E. A. Davis, *Electronic Processes in Non-Crystalline Materials,* 2nd ed. (Oxford University, London, 1979).
[3]D. J. Thouless, Phys. Rep. C **13**, 93 (1974).
[4]E. Abrahams, P. W. Anderson, D. C. Licciardello, and T. V. Ramakrishnan, Phys. Rev. Lett. **42**, 673 (1979).
[5]D. Vollhardt and P. Woelfle, Phys. Rev. Lett. **45**, 482 (1980); F. J. Wegner, Z. Phys. B **35**, 207 (1979).
[6]M. Kaveh and N. F. Mott, J. Phys. C **18**, 2235 (1983).
[7]Roger Haydock, Philos. Mag. B **43**, 203 (1981); **53**, 554 (1986).
[8]Roger Haydock, in *Solid State Physics,* edited by H. Ehrenreich, F. Seitz, and D. Turnbull (Academic, New York, 1980), Vol. 35, p. 215.
[9]For example, A. MacKinnon and B. Kramer, Phys. Rev. Lett. **47**, 1546 (1981); G. M. Scher, J. Non-Cryst. Solids **59-60**, 33 (1983); H. de Raedt, Comp. Phys. Rep. **7**, 1 (1987).
[10]T. J. Godin and Roger Haydock, Europhys. Lett. **14**, 137 (1991).
[11]T. J. Godin and Roger Haydock, Phys. Rev. B **38**, 5237 (1988).
[12]T. J. Godin and Roger Haydock, Comput. Phys. Commun. **64**, 123 (1991).
[13]C. C. Paige, J. Inst. Math. Appl. **10**, 372 (1972); B. N. Parlett, *The Symmetric Eigenvalue Problem* (Prentice Hall, Englewood Cliffs, NJ, 1980).
[14]I. M. Lifschitz, Zh. Eksp. Teor. Fiz. **44**, 1780 (1963) [Sov. Phys. JETP **17**, 1195 (1963)].
[15]Bogdan Bulka, Bernhard Kramer, and Ludwig Schweitzer, J. Non-Cryst. Solids **77-78**, 29 (1985).